



## Supporting Online Material for

### **Phase Transitions of Dirac Electrons in Bismuth**

Lu Li,\* J. G. Checkelsky, Y. S. Hor, C. Uher, A. F. Hebard, R. J. Cava, N. P. Ong\*

\*To whom correspondence should be addressed. E-mail: luli@princeton.edu (L.L.);  
npo@princeton.edu (N.P.O.)

Published 25 July 2008, *Science* **321**, 547 (2008)

DOI: 10.1126/science.1158908

#### **This PDF file includes:**

Materials and Methods  
SOM Text  
Figs. S1 to S6  
References

# Supporting Online Material: Phase transitions of Dirac electrons in bismuth

Lu Li<sup>1</sup>, J. G. Checkelsky<sup>1</sup>, Y.S. Hor<sup>2</sup>, C. Uher<sup>3</sup>, A. Hebard<sup>4</sup>, R. J. Cava<sup>2</sup> and N. P. Ong<sup>1</sup>  
*Departments of Physics<sup>1</sup> and Chemistry<sup>2</sup>, Princeton University, New Jersey 08544, U.S.A.*  
*Department of Physics<sup>3</sup>, Univ. of Michigan, Ann Arbor, Michigan 48109, U.S.A.*  
*Department of Physics<sup>4</sup>, Univ. of Florida, Gainesville, Florida 32611, U.S.A.*

(Dated: May 30, 2008)

## I. METHODS AND MATERIALS

### A. Torque magnetometry

We extend the standard analyses of magnetization (usually in the low-field regime [S1, S2, S3, S4]) to obtain explicit forms for the torque at the quantum limit with  $n = 1, 2, \dots$  for an ellipsoidal FS in an oblique magnetic field  $\mathbf{H}$ .

The free energy  $\mathcal{F}$  at temperature  $T = 0$  is the sum over occupied Landau levels  $n$ , viz. [S1]

$$\mathcal{F} = -\frac{g}{2\pi\ell_B^2} \sum_n \int_{-\kappa_n}^{\kappa_n} \frac{d\kappa}{2\pi} [\mu - \epsilon_n(\theta, \kappa)], \quad (\text{S1})$$

where  $g$  is the degeneracy of each level,  $\mu$  the chemical potential,  $\ell_B = \sqrt{\hbar/eB}$  the magnetic length,  $e$  the electron charge and  $2\pi\hbar$  is Planck's constant. The energy of the  $n^{\text{th}}$  Landau level (LL)  $\epsilon_n(\theta, \kappa)$  is sensitive to the tilt angle  $\theta$  of  $\mathbf{H}$ . The limits  $\pm\kappa_n$  of the integral over  $\kappa$  (the component of the wavevector  $\mathbf{k}$  parallel to  $\mathbf{H}$ ) are set by the occupied states. For simplicity, we consider quadratic dispersion in zero  $H$  given by

$$\epsilon(\mathbf{k}) = \frac{\hbar^2}{2} \left[ \frac{k_x^2}{m_1} + \frac{k_y^2}{m_2} + \frac{k_z^2}{m_3} \right]. \quad (\text{S2})$$

We specialize to the prolate case  $m_1 = m_2 \ll m_3$ , with  $\mathbf{H}$  nearly aligned with the  $z$  axis (Fig. S1 inset). The heavy mass is along the field direction, and the highest cyclotron frequency occurs for orbits in the plane normal to  $\mathbf{H}$ . In bismuth, this applies to the hole ellipsoid with  $\mathbf{H}$  nearly aligned with the trigonal axis.

First, for  $\theta = 0$ , the Landau-level spectrum is

$$\epsilon_n(\kappa) = (n + \gamma)\hbar\omega_c + \frac{\hbar^2\kappa^2}{2m_3}, \quad (\text{S3})$$

where  $\omega_c = eB/m_2$  and  $\gamma$  is the Onsager phase. This fixes  $\kappa_n$  to be

$$\frac{\hbar^2\kappa_n^2}{2m_3} = \mu - (n + \gamma)\hbar\omega_c. \quad (\text{S4})$$

The free energy may be evaluated to give [S3]

$$\mathcal{F} = -\frac{g}{3\pi^2\ell_B^2} \frac{\sqrt{2m_3}}{\hbar} \sum_{n=0}^{n_M} [\mu - (n + \gamma)\hbar\omega_c(\theta)]^{\frac{3}{2}}, \quad (\text{S5})$$

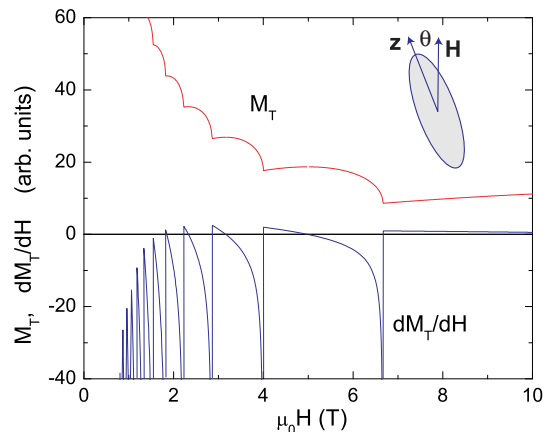


FIG. S1: The torque calculated from Eq. S7 displayed as the transverse magnetization  $M_T = \tau/VH$  vs.  $H$  (red curve) at a fixed, positive  $\theta$ . The derivative  $\partial M_T/\partial H$  is shown in blue.  $\mu$  is assumed to be  $H$  independent. Level broadening of the LLs is assumed to be zero. The inset shows the sample axis  $\hat{\mathbf{z}}$  tilted by  $\theta$  relative to  $\mathbf{H}$ .

with  $n_M$  the largest integer for which

$$\mu - (n + \gamma)\hbar\omega_c > 0. \quad (\text{S6})$$

Next, we consider a small tilt angle  $\theta$ . We regard  $\theta$  as the angular coordinate of the sample relative to  $\mathbf{H}$  which is fixed in the lab frame (Fig. S1 inset). Treating  $\theta$  as a perturbation to second order (and rotating the quantization axis), one finds [S8] that the largest effect is to change  $\omega_c(\theta)$  in the summand (the effect on  $m_3(\theta)$  outside the sum is negligible by comparison). The torque  $\tau$  is the derivative  $-\partial\mathcal{F}/\partial\theta$ . Differentiating Eq. S5, we have

$$\tau = +\frac{g\theta\omega_c}{4\pi^2\ell_B^2} \sqrt{2m_3} \sum_{n=0}^{n_M} [\mu - (n + \gamma)\hbar\omega_c]^{\frac{1}{2}} (n + \gamma). \quad (\text{S7})$$

The positive sign implies that the torque acts in the same direction as the tilt of the sample, tending to rotate the sample axis farther from alignment with  $\mathbf{H}$ . The ellipsoid with  $\mathbf{H}||\hat{\mathbf{z}}$  is unstable with respect to a weak tilting (as discussed below).

The torque calculated from Eq. S7 is plotted as a transverse magnetization  $M_T = \tau/VH$  vs.  $H$  in Fig. S1, together with its derivative  $\partial M_T/\partial H$  ( $V$  is the volume and  $H = |\mathbf{H}|$ ). Level broadening is neglected and  $\mu$  is

taken to be  $H$ -independent. We note that the peaks are negative-pointing minima when  $M_T$  is positive (and vice versa).

To illuminate the sign of  $M_T$ , it is helpful to re-express Eq. S7 in terms of a magnetic moment generated by the orbital current. The electron population  $N_n$  in the  $n^{\text{th}}$  LL is obtained by integrating the density of states from  $(n + \gamma)\hbar\omega_c$  to  $\mu$ . We have

$$N_n = \frac{g}{2\hbar\pi^2\ell_B^2} \sqrt{2m_3} [\mu - (n + \gamma)\hbar\omega_c]^{\frac{1}{2}}. \quad (\text{S8})$$

The current  $I_n = N_n|e|\omega_c/2\pi$  multiplied by the orbit area gives the magnitude of the diamagnetic moment when summed over  $n$ . In  $\mathbf{k}$ -space the radius  $k_{\perp,n}$  of the quantized orbits (in the plane normal to  $\mathbf{H}$ ) is obtained by equating

$$\frac{\hbar^2 k_{\perp,n}^2}{2m_2} = (n + \gamma)\hbar\omega_c. \quad (\text{S9})$$

From the area in  $\mathbf{k}$  space,  $S = \pi k_{\perp,n}^2$ , we obtain the area  $A_n$  of the quantized orbits in real space

$$A_n = S\ell_B^4 = \frac{2\pi m_2}{\hbar} (n + \gamma)\omega_c \ell_B^4. \quad (\text{S10})$$

With Eqs. S8, S10, we write the torque as  $\vec{\tau} = \sum_n \mathbf{m}_n \times \mathbf{H}$ , with the moment of the  $n^{\text{th}}$  LL given by

$$\mathbf{m}_n = -N_n|e|\frac{\omega_c}{2\pi} A_n \hat{\mathbf{z}}. \quad (\text{S11})$$

Comparing with Eq. S7, we see that this accounts for all the factors except for a factor  $\frac{1}{2}$ , which comes from the derivative  $\partial S/\partial\theta$  and cannot be captured with this argument. Aside from this difference, the ‘‘moment’’ description identifies the origin of each of the factors in Eq. S7. In particular, it shows physically that the diamagnetic orbital currents lead to a moment antiparallel to  $\mathbf{H}$  which, for a small tilt, produces an unstable torque. Moreover, for the lowest LL ( $n = 0$ ), Eq. S11 reduces to (correcting for the factor  $\frac{1}{2}$ )

$$\mathbf{m}_0 = -N_0\mu_B \frac{m_e}{m_2} \gamma \hat{\mathbf{z}}, \quad (\text{S12})$$

with  $\mu_B = e\hbar/2m_e$  the Bohr magneton and  $m_e$  the free electron mass. The moment of each electron is of the order of the Bohr magneton  $\mu_B$  enhanced by the inverse effective mass ratio. Hence, in this geometry, the transverse magnetization in the quantum limit is

$$M_T^{(n=0)} = +\frac{N_0 m_e}{V m_2} \mu_B \gamma \sin\theta. \quad (\text{S13})$$

The  $+$  sign means that  $M_T$  has the same sign as  $\theta$ . Hence if  $\mathbf{H} \times \mathbf{z} \parallel \mathbf{x}$  (as drawn in Fig. 1 of main text), the torque  $\mathbf{m}_0 \times \mathbf{H}$  is also  $\parallel \mathbf{x}$ , consistent with a moment direction along  $-\mathbf{z}$ . The ellipsoid is unstable to a slight tilt of  $\mathbf{H}$  away from the long axis. This applies to the

hole ellipsoid in bismuth for  $\mathbf{H} \parallel \mathbf{z}$  (the trigonal axis). However, the electron ellipsoids lie nominally in the  $\mathbf{x}$ - $\mathbf{y}$  (bisectrix-binary) plane, with their long axes nominally at an angle  $90^\circ \pm \beta$  to  $\mathbf{H}$  ( $\beta \sim 6.5^\circ$ ). For small tilt angle  $\theta$ , the electron FS torques are large, and act in a direction opposite to  $\mathbf{H} \times \mathbf{z}$ . Hence, the dominance of the electron ellipsoids over the holes implies that  $M_T$  is opposite in sign to  $\theta$  in bismuth (when  $\mathbf{H}$  is nearly parallel to the trigonal axis).

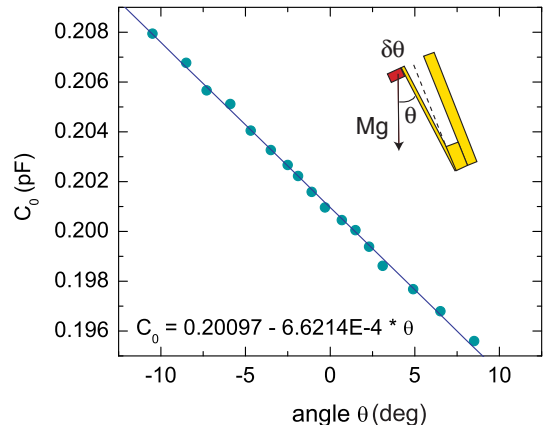


FIG. S2: Calibrating the cantilever by weighing the sample in  $\mathbf{H} = \mathbf{0}$ . The inset shows the deflection angle  $\delta\theta$  of the cantilever arm caused by the weight  $Mg$  of the sample (red). The thick yellow strip is the rotatable platform viewed edgewise. The deflection angle (measured as a change in capacitance  $C_0$ ) is observed to change linearly with  $\theta$  in agreement with Eq. S14. The slope allows  $K$  to be calculated in absolute units. At the largest tilt, the deflection  $\delta\theta_{max} < 0.1^\circ$ .

## B. Calibrating the cantilever

To convert the observed torque into absolute units, we need to know the torsion spring constant  $K$  of the cantilever. A convenient technique is to use the cantilever to ‘‘weigh’’ the sample in zero  $\mathbf{H}$  at different tilt angles  $\theta$  of the sample/platform to the vertical (lab) axis. Under gravity, the torque  $Mg\ell \sin\theta$  is counter-balanced by  $K\delta\theta$ , with  $Mg$  the weight,  $\ell$  the cantilever length and  $\delta\theta$  the (small) angular deflection of the cantilever (inset, Fig. S2). The fractional change in capacitance  $\delta C/C_0$  is given by

$$\frac{\delta C}{C_0} = -\frac{Mg\ell^2 \sin\theta}{Kd}, \quad (\text{S14})$$

where  $d$  is the zero-torque capacitance gap.

A complication is that the observed capacitance includes a large background contribution  $C_b$  from the gold wires contacting the capacitor. When  $\theta$  is set to a new value,  $C_b$  also changes because of slight flexing of the wires. This would require a separate calibration at each value of  $\theta$ . To remove this complication, we used flexible coax cables throughout, for which  $C_b$  is small and

insensitive to changes in  $\theta$ . With this improvement, the observed  $\delta C$  is strictly linear in  $\theta$  (Fig. S2). This allows  $K$  to be measured directly. The crystal Sample 1 is of dimension 5.25 mm  $\times$  1.50 mm  $\times$  1.55 mm and mass 0.12 g. The cantilever arm has dimensions  $\ell = 5.8$  mm, width  $w = 1.1$  mm and thickness  $t = 50$   $\mu$ m, while the capacitor spacing  $d = 0.5$  mm. From the slope of the line in Fig. S2, the measured value of  $K = 4.2 \times 10^{-4}$  Nm/rad, which is slightly smaller than the calculated value  $4.9 \times 10^{-4}$  Nm/rad. The cantilever, which can resolve a moment of  $10^{-11}$  J/T, is sufficiently stiff that its deflection is  $< 0.5^\circ$  even at 31 T.

## II. MAGNETIZATION RESULTS IN BISMUTH

In the past, the LL's arising from the electron FS ellipsoids were essentially "invisible" in both dHvA and SdH (Shubnikov-de Haas) experiments when  $\mathbf{H}$  is near alignment with the trigonal axis  $\mathbf{z}$  [S4, S5, S6, S7]. One difficulty is that, in this field geometry, the cross-section areas of the projected hole and electron FS are nearly equal, which renders Fourier analyses of the multiple oscillations in weak fields ineffective. A second reason is that the holes dominate the Hall and longitudinal resistivities  $\rho_{xy}$  and  $\rho_{xx}$ , effectively obscuring the contribution of the electron ellipsoids to the transport signal (quantum oscillations of the latter are virtually unresolved in SdH experiments). Extensive search of the literature reveals that all previous magnetization and torque experiments were confined to low  $H$  ( $< 2$  T) [S2, S3, S4, S5].

In our torque experiment, tilting  $\mathbf{H}$  in the  $yz$  plane lifts the symmetry between the 3 electron ellipsoids (see inset of Fig. 1A, main text). By design, the cantilever responds only to the  $x$  component of  $\vec{\tau}$ . Thus, it is most sensitive to the competing torques arising from electron ellipsoids 2 and 3. For a FS ellipsoid with major axis  $\hat{\mathbf{e}}$ , the magnetization in the semiclassical regime is  $\mathbf{M} = \mathbf{H} \cdot \hat{\mathbf{e}} \chi_{\parallel} + (\mathbf{H} - \mathbf{H} \cdot \hat{\mathbf{e}}) \chi_{\perp}$ , where  $\chi_{\parallel}$  ( $\chi_{\perp}$ ) is the susceptibility measured with  $\mathbf{H} \parallel \hat{\mathbf{e}}$  ( $\mathbf{H} \perp \hat{\mathbf{e}}$ ). The  $x$  components of the torque arising from the electron ellipsoids 2 and 3 are, respectively (for  $\beta \ll 1$  and  $\theta \ll 1$ )

$$\tau_2 = \Delta\chi_e H^2 (\beta + w\theta)w,$$

$$\tau_3 = -\Delta\chi_e H^2 (\beta - w\theta)w,$$

with  $\beta$  the tilt-angle of each ellipsoid out of the  $xy$  plane, and  $w = \cos(\pi/6)$ . The torque from the hole ellipsoid is

$$\tau_{hole} = -\Delta\chi_h H^2 \theta, \quad (\text{S15})$$

while the torque from ellipsoid 1 is

$$\tau_1 = -\Delta\chi_e H^2 \theta \beta^2. \quad (\text{S16})$$

Here,  $\Delta\chi_{e,h} = \chi_{\parallel} - \chi_{\perp}$  for the electron and hole ellipsoids, respectively. With  $\beta \simeq 6.5^\circ$ ,  $\tau_1$  is 70 times weaker than the hole signal, which is in turn 2-10 times weaker

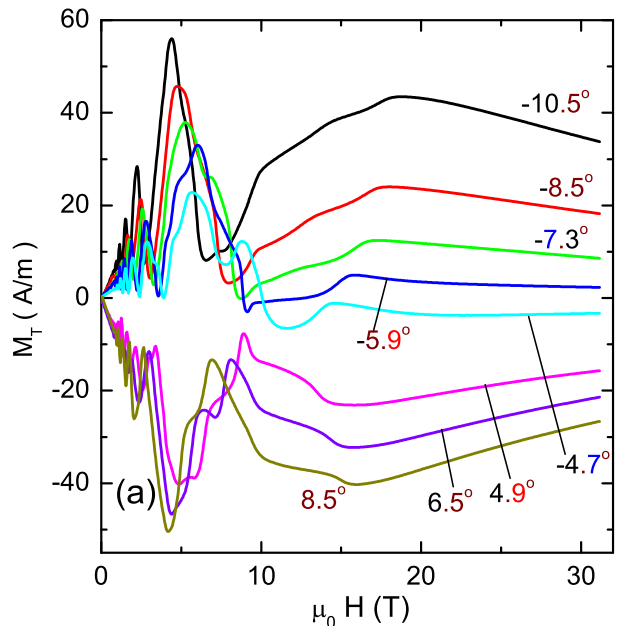


FIG. S3: Curves of transverse magnetization  $M_T = \tau/VH$  vs.  $H$  at tilt angles outside the critical window ( $|\theta| > 4^\circ$  measured at 0.3 K. Curves inside the window are shown in Fig. 1 of main text. The crossing of Landau levels past  $\mu$  lead to strong oscillations in  $M_T$  below 10 T. Above 10 T, some sublevels remain visible. The "knee" at 17.5 T in the upper-most curve ( $\theta = -10.5^\circ$ ) is the sublevel (0,-) (see Fig. 3 in main text).

than  $\tau_2$  and  $\tau_3$  when  $|\theta| < 2^\circ$ . This "filtering" allows us to concentrate only on the Dirac electrons in ellipsoids 2 and 3.

Figure S3 shows curves of the transverse magnetization  $M_T$  vs.  $H$  for tilt angles  $\theta$  outside the critical window in which the transitions at  $H_1$  and  $H_2$  occur. First, we note that the sign of  $M_T$  is positive if  $\theta$  is negative (i.e. opposite to that in Eq. S13), because the electron FS ellipsoids dominate the torque signal. We define the angle  $\theta$  to be positive if  $\mathbf{H} \times \mathbf{z} \cdot \mathbf{x} > 0$  (as in inset of Fig. 1A). At low  $H$ , the quantum oscillations from the LL crossings dominate  $M_T$ . Some sublevels may be seen directly in  $M_T$ . The highest sublevel (0,-) is apparent as the "knee" feature at 17.5 T in the uppermost curve ( $\theta = -10.5^\circ$ ). As  $\theta$  increases to  $-4.7^\circ$ , it decreases to 13 T.

The strong dispersion of the quantum oscillation in  $\partial M_T / \partial H$  is apparent in Fig. S4 which displays the derivative curves at 6 angles inside the critical window  $|\theta| < 4^\circ$ . The data are from the low-field set. By plotting the peak fields  $B_n$  in the plane of  $H$  vs.  $\theta$  (Fig. 2 of main text), we confirm that they vary strongly with  $\theta$ . By contrast, the hole line at  $n = 1$  remains nearly  $\theta$ -independent at  $H = 9.15$  T. In all the panels, the feature at the highest field is the transition field  $H_1$ .

Figure S5 provides an expanded view of the curves  $\partial M_T / \partial H$  in the region of  $H_1$ . As  $\theta$  decreases from  $7.8^\circ$

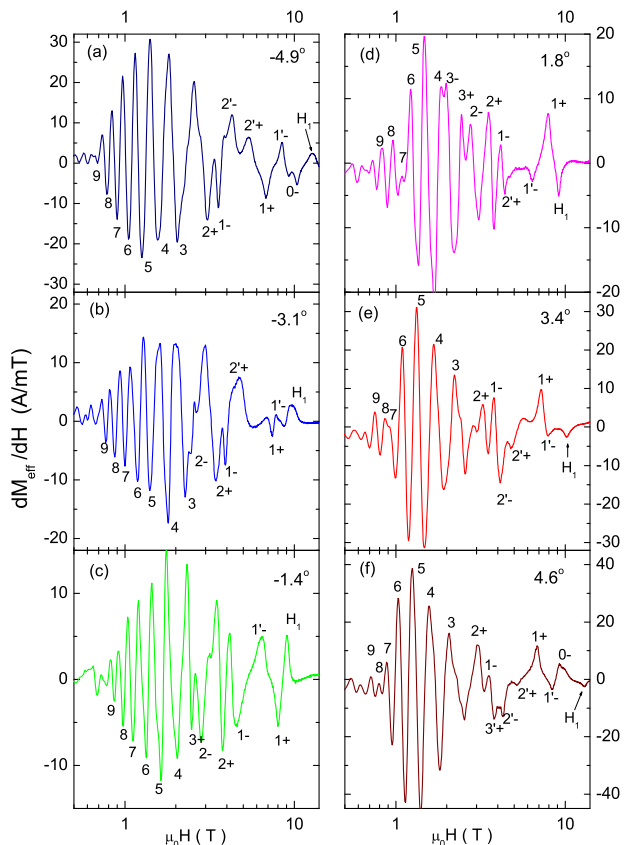


FIG. S4: The derivative of the transverse magnetization  $\partial M_T/\partial H$  vs.  $H$  at 6 selected values of  $\theta$  taken at  $T = 1.5$  K ( $H$  is in log scale). For  $\theta < 0$  (Panels a-c),  $\tau > 0$ . Crossings of the Landau sublevels ( $n, s$ ) appear as minima in  $\partial M_T/\partial H$ , as labelled. If the sublevels disperse pass  $\theta = 0$ , they become maxima (and are flagged by a prime on  $n$ ). For  $\theta > 0$  (d-f), the reverse holds. At low  $H$ , the label  $n$  is short hand for the sublevel ( $n, +$ ), which is degenerate with ( $n - 1, -$ ) (see Sec. IV). The transition field  $H_1$  is apparent in all panels as the peak at the highest field (as marked).

to  $6^\circ$  (lowest 3 curves), the hole anomaly remains at 9.15 T but fades in amplitude (vertical dashed line). At  $\theta = 4.6^\circ$ , the  $H_1$  anomaly is seen at 13 T. With decreasing  $\theta$ , it moves rapidly to lower  $H$ , as tracked by the grey curve. The latter intersects the hole line near  $1.8^\circ$ . The strongly dispersing peaks correspond to the electron sublevels (0,-) and (1,+), as labelled. We note that all these peaks vanish when they cross the grey curve into the “quiet” cone region (upper right corner).

### III. THE COHEN-BLOUNT MODEL

Extensive magneto-optics experiments [S9, S10] in the 60’s and 70’s have shown that the electron ellipsoids are accurately described by the Dirac Hamiltonian. In zero

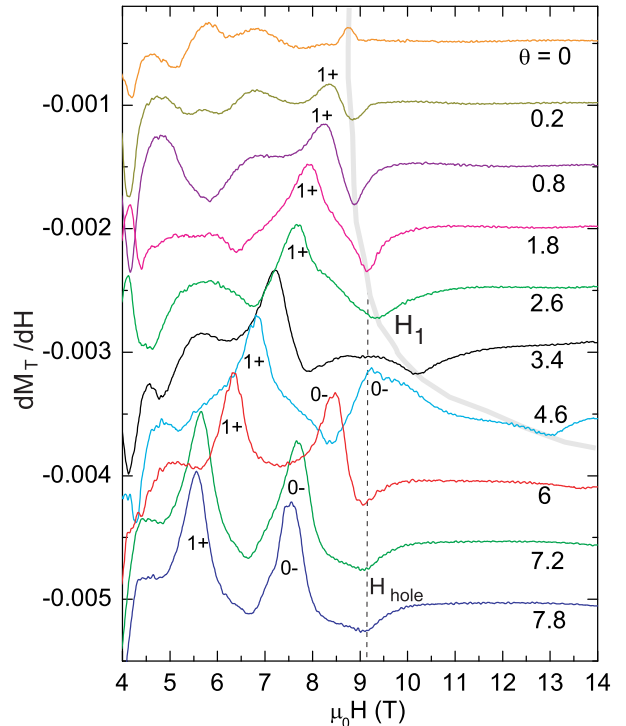


FIG. S5: Curves of the transverse-magnetization derivative  $\partial M_T/\partial H$  vs.  $H$  at 10 angles  $\theta \geq 0$  taken at  $T = 1.5$  K (displaced vertically for clarity). The grey curve (upper right corner) traces the dispersion of  $H_1$  vs.  $\theta$ . The vertical dashed line tracks the hole sublevel at 9.15 T (its amplitude decreases as  $\theta$  decreases below  $4^\circ$ ). The grey curve intersects the vertical line near  $1.8^\circ$ . The peaks representing the sublevels (0,-) and (1,+), as labelled, disperse strongly, but vanish when they cross the grey curve.

$H$ , it is given by [S11, S9, S12]

$$\mathcal{H} = \frac{E_G}{2} \tilde{\beta} + \frac{\hbar^2 \Delta \mathbf{k}^2}{2m} \tilde{1} + i \Delta \mathbf{k} \cdot \mathbf{W}(i) \tilde{\beta} \tilde{\alpha}_i, \quad (\text{S17})$$

where  $\Delta \mathbf{k} = \mathbf{k} - \mathbf{k}_0$  is the wavevector measured from the ellipsoid center (at L), and  $E_G$  is the mass gap. The 3 vectors  $\mathbf{W}(i)$  ( $i = 1, 2, 3$ ) are velocity matrix elements which strongly admix spin- $\uparrow$  and spin- $\downarrow$  states. The wave function  $\Psi = |\psi_{c,\uparrow}, \psi_{c,\downarrow}, \psi_{v,\uparrow}, \psi_{v,\downarrow}\rangle$  has 4 components reflecting the conduction and valence bands and the 2 spin states. In Eq. S17, the  $4 \times 4$  Dirac matrices  $\tilde{\beta}$  and  $\tilde{\alpha}_\mu$  are defined as

$$\tilde{\beta} = \begin{bmatrix} 1 & 0 \\ 0 & -1 \end{bmatrix}, \quad \tilde{\alpha}_i = \begin{bmatrix} 0 & \sigma_i \\ \sigma_i & 0 \end{bmatrix}, \quad (\text{S18})$$

with  $\sigma_i$  the  $2 \times 2$  Pauli matrices.

In finite field, we replace  $\Delta \mathbf{k} \rightarrow \tilde{\pi} = (\Delta \mathbf{k} - e \mathbf{A})$  with  $\mathbf{A}$  the vector potential. Neglecting the kinetic energy term  $\hbar^2 \Delta \mathbf{k}^2 / 2m$ , we may diagonalize Eq. S17 (this approximation is most appropriate for  $\mathbf{H} \parallel \hat{x}$ , the bisectrix axis). The energies of the Landau levels are then of the Dirac

form, viz. [S12, S13]

$$E_{n,s} = \pm \sqrt{\left(\frac{E_g}{2}\right)^2 + E_G \left[ \left(n + \frac{1}{2} - \frac{s}{2}\right) \hbar \omega_c \right]}, \quad (\text{S19})$$

where  $+(-)$  applies to the conduction (valence) band, and  $s = \pm 1$  indexes the Kramer's doublet,  $\omega_c \sim 1/E_g$  the cyclotron frequency [S12]. Because of the very large spin-orbit energy ( $\sim 1$  eV), the effective magnetic moment  $\vec{\mu} = \vec{\mu}_s + \vec{\mu}_{orb}$  is the sum of a small spin moment  $\vec{\mu}_s$  and a dominant orbital moment  $\vec{\mu}_{orb}$  [S11]. The  $H$  dependence of Eq. S19 is shown in the inset of Fig. S6. We note that the sublevels  $(n-1, -)$  and  $(n, +)$  are degenerate for  $n \neq 0$ . However, the lowest sublevel  $(0, +)$  is non-degenerate and independent of  $H$  (this is the much-discussed zero-energy mode of the Dirac spectrum).

#### IV. INDEXING OF LANDAU LEVELS

The LL indexing shown in Figs. 2 and 3 are obtained from comparing the measured index fields  $B_{n,s}$  with the Dirac spectrum. A test for the correct indexing of the Landau sublevels is obtained by plotting the reciprocal of the peak fields  $B_n$  against the integers. By the usual quantization condition, the fields  $B_n(\theta)$  are given by (we suppress the  $s$  index)

$$\frac{1}{B_n(\theta)} = \frac{2\pi e}{\hbar} [n + \gamma] \frac{1}{S(\theta)}, \quad (n = 0, 1, 2, \dots), \quad (\text{S19})$$

where  $S(\theta)$  is the FS cross-section area projected onto the plane normal to  $\mathbf{H}$ .

Values of  $B_{n,s}$  measured at the angle  $\theta = -4.6^\circ$  for  $s = \pm 1$  are plotted in Fig. S6 in the range  $0 < n \leq 10$ . The former (blue circles) falls on a straight line extrapolating to the origin as  $H \rightarrow \infty$ , whereas the latter (magenta) initially lies on the dashed line, but deviates slightly at large  $H$ . From the slope of the solid line, the area  $S_e = 6.21$  T. The linear variation of  $1/B_n$  vs.  $n$  confirms that the relative indexing is consistent. Moreover, the ability to reach the last few sublevels in intense fields allows us to test the absolute indexing. We now discuss the features in detail.

As discussed, the Dirac spectrum [S11, S12] Eq. S19 has the “shifted  $n$ ” indexing by which  $(n-1, -)$  and  $(n, +)$  are degenerate for  $n \neq 0$ .

Our measured  $B_n$ 's confirm this shifted indexing. As shown in Fig. S6, the sublevels  $(n, +)$  (blue circles) fall on a straight line passing through the origin. Interestingly, the sublevels  $(n, -)$  (magenta circles) initially follow the (dashed) line intercepting the  $n$  axis at -1 in accord with Eq. S19. For  $H > 2$  T, however, lifting of the degeneracy becomes resolvable. As  $H$  increases,  $1/B_n$  deviates from the dashed line to intercept the  $n$  axis at -0.6 (solid magenta line). The high-field deviation may involve terms neglected in the models of Cohen and Blount [S11] and Wolff [S12].

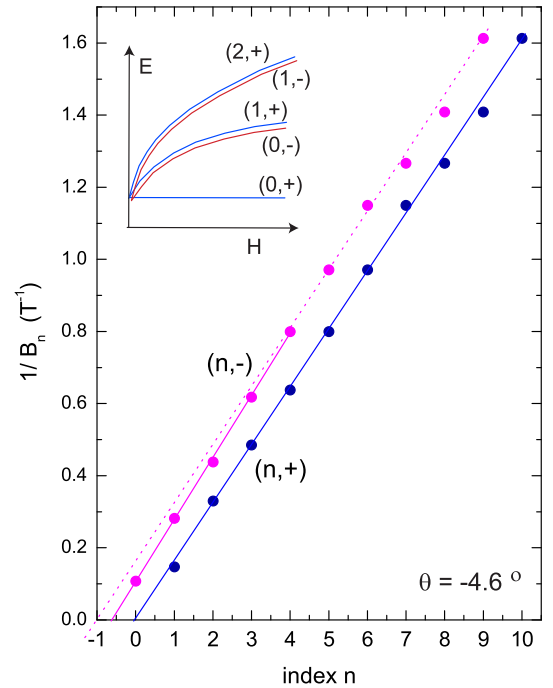


FIG. S6: Plot of the observed  $1/B_n$  vs. the integers  $n$  for the doublets  $s = \pm 1$ . The sublevels  $(n, +)$  (blue circles) fall on a straight line passing through the origin. The slope gives an area  $S_e = 6.21$  T. At low  $H$ , the sublevels  $(n, -)$  (magenta) fall on the dashed line (parallel to the blue line, but intercepting the  $n$  axis at -1). Above 2 T, they deviate to follow the solid magenta line, which intercepts the  $n$  axis at  $n = -0.6$ . The inset shows the Dirac spectrum  $E$  vs.  $H$  (Eq. S19) [S11, S12]. For finite  $n$ , the sublevels  $(n-1, -)$  and  $(n, +)$  are degenerate (red and blue curves). However, the zero-energy sublevel  $(0, +)$  is  $H$  independent and non-degenerate.

Aside from this deviation, the measured  $B_{n,s}$  support the spectrum of Eq. S19. In particular, the last 2 sublevels to be “emptied” are  $(1, +)$  and  $(0, -)$ . No further sublevels are observed up to our highest field of 31 T. This leaves the last sublevel  $(0, +)$  to “pin” the chemical potential.

We have also tested the more conventional indexing scheme  $(n', s')$  in which 2 sublevels are identified with the same  $n'$  if they are degenerate or nearly so. In that scheme, we should re-label

$$(n, +) \rightarrow (n', -), \quad (n-1, -) \rightarrow (n', +), \quad (\text{S20})$$

so that  $(n', +)$  is degenerate with  $(n', -)$  at low  $H$ . (In Fig. S6, this involves shifting each magenta circle to the right by one integer.) However, this conventional scheme runs into serious difficulties in the large- $H$  limit ( $n \leq 1$ ). The sublevel  $(n', s') = (0, -)$  is reached in the limit  $H \rightarrow \infty$ , but the sublevel  $(n', s') = (0, +)$  occurs at a *negative* value of  $1/B_n$ , which is unphysical. This conceptual difficulty is a strong argument favoring the shifted Dirac indexing.

- 
- [S1] I. M. Lifshitz, A. M. Kosevich, Zh. Eksperim. i Teor. Fiz. **29**, 730 (1955) [Sov. Phys. JETP **2**, 636 (1956)].
- [S2] D. Shoenberg, *Magnetic oscillations in metals* (Cambridge University Press, 1984).
- [S3] D. Shoenberg, J. Phys. F **18**, 499 (1988).
- [S4] R. N. Bhargava, Phys. Rev. **156**, 785 (1967).
- [S5] Rodney D. Brown, III, Phys. Rev. B **2**, 928 (1970).
- [S6] F. Y. Yang *et al.*, Phys. Rev. B **61**, 6631 (2000).
- [S7] S. G. Bompadre, C. Biagini, D. Maslov, A. F. Hebard, Phys. Rev. B **64**, 073103 (2001).
- [S8] N. P. Ong, unpublished.
- [S9] R. N. Brown, J. G. Mavroides, and B. Lax, Phys. Rev. **129**, 2055 (1963)
- [S10] Martin Maltz and M. S. Dresselhaus, Phys. Rev. B **2**, 2877 (1970)
- [S11] M. H. Cohen, E. I. Blount, Phil. Mag. **5**, 115 (1960).
- [S12] P. A. Wolff, J. Phys. Chem. Solids **25**, 1057 (1964).
- [S13] H. Fukuyama, R. Kubo, J. Phys. Soc. Jpn. **28**, 570 (1970).